







RESEARCH ARTICLE | FEBRUARY 24 2023

## Head-on collision of unequal-size droplets on a wetting surface

Saroj Ray ; Yicheng Chi (池亦承) ; Peng Zhang (张鹏)  ; Song Cheng (成松)  



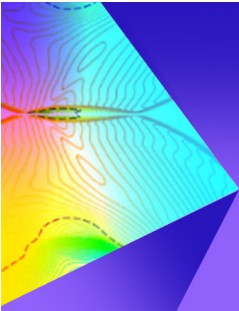
*Physics of Fluids* 35, 022114 (2023)

<https://doi.org/10.1063/5.0139663>



Export  
Citation

CrossMark



## Physics of Fluids

### Special Topic: Shock Waves

Submit Today!

# Head-on collision of unequal-size droplets on a wetting surface

Cite as: Phys. Fluids **35**, 022114 (2023); doi: [10.1063/5.0139663](https://doi.org/10.1063/5.0139663)

Submitted: 22 December 2022 · Accepted: 6 February 2023 ·

Published Online: 24 February 2023



View Online



Export Citation



CrossMark

Saroj Ray,<sup>1</sup> Yicheng Chi (池亦承),<sup>2</sup> Peng Zhang (张鹏),<sup>2,a)</sup> and Song Cheng (成松)<sup>1,a)</sup>

## AFFILIATIONS

<sup>1</sup>Department of Mechanical Engineering, The Hong Kong Polytechnic University, Kowloon, Hong Kong

<sup>2</sup>Department of Mechanical Engineering, City University of Hong Kong, Kowloon Tong, Kowloon, Hong Kong

<sup>a)</sup>Authors to whom correspondence should be addressed: [penzhang@cityu.edu.hk](mailto:penzhang@cityu.edu.hk) and [songryan.cheng@polyu.edu.hk](mailto:songryan.cheng@polyu.edu.hk)

## ABSTRACT

Impacts of liquid droplets with another stationary droplet resting on a surface are important basic processes in many applications such as agricultural sprays, spray cooling, and inkjet printing. We investigated the head-on collision of unequal-size droplets of the same liquid on wetting surfaces both experimentally and theoretically at different size ratios and low-impact Weber numbers ( $We$ ). A series of high-speed camera images showing representative sequences of collision processes for greatly different size ratios are analyzed. Different collision outcomes such as coalescence, bouncing, and partial coalescence–partial bouncing are analyzed thoroughly. Four different stages are identified for characterizing the complete bouncing process during the impact of unequal-size droplets on a solid surface. Subsequently, an analytical model based on energy balance is developed to calculate the maximum spread diameter and restitution coefficient of falling droplets, and compared with experimental data, satisfactory qualitative agreements are obtained. Results show that the dimensionless maximum spread diameter of falling droplets depends weakly on  $We$  and it is small for a higher size ratio. The restitution coefficient does not change significantly at a higher size ratio at a fixed  $We$  despite more viscous dissipation in bigger sessile droplets and it scales with  $We^{-1/2}$ .

Published under an exclusive license by AIP Publishing. <https://doi.org/10.1063/5.0139663>

## I. INTRODUCTION

A fundamental understanding of drop-on-drop impacts where the impact of a moving droplet with another droplet sitting on a solid surface occurs is crucial for several applications. A prominent example is the spraying of pesticides on plants in agriculture, where the expelled droplets may collide with the previously sprayed droplets, dew, or rainwater on leaves. In that case, it is essential to know whether the colliding droplet stays attached or bounces away and falls on the soil to cause contamination.<sup>1–3</sup> In inkjet printing, multiple droplets might be ejected onto a paper to generate a single dot of an image. The spreading of the droplets is important to obtain sharp images, and predicting the maximum spread diameter can help optimize the printing parameters.<sup>4–6</sup>

In the past, binary droplet collision had been explored extensively. Early experimental studies performed with water at atmospheric pressure discovered two distinct collision outcomes: permanent droplet coalescence and droplet separation after temporary coalescence.<sup>7,8</sup> It was found that the collision outcomes are mainly affected by the collision Weber number (defined as  $We = \rho U^2 D / \sigma$  for droplets with equal size, where  $\rho$ ,  $U$ ,  $D$ , and  $\sigma$  are density, relative impact velocity, droplet diameter, and surface tension, respectively), which measures

the relative importance of the droplet inertia compared to the surface tension, and the impact parameter,  $B$ , which measures the deviation of droplet colliding trajectory from that of an exact head-on collision. Binary droplet collision of alkane droplets was investigated by Jiang *et al.*<sup>9</sup> They observed that droplet bouncing occurs at low  $We$  ( $O(1)$ ) and separation with satellite droplet(s) formation (referred to as reflex separation regime) at moderately higher  $We$  ( $O(10)$  and above). They found that, for the droplets to coalesce, the air layer between them must be drained out and the interfaces of droplets must come very close to each other (e.g., on the order of 100 nm), while bouncing occurs because the pressure buildup in the air layer is great enough to push the droplets away before air can drain out completely. Subsequently, the well-known collision nomogram was put forth in the  $We$ – $B$  parameter space by Qian and Law.<sup>10</sup> They observed stretched droplet separation at high  $B$  values and suggested that differences in viscosity and surface tensions caused the different collision behavior between water and hydrocarbon droplets. They also corroborated that increasing ambient pressure promotes droplet bouncing. More complex behaviors are encountered for droplet collisions at high  $We$  numbers or with droplets of different liquids. For instance, droplet collision at  $We > 200$  can cause droplet splattering,<sup>11</sup> and collisions

with dissimilar liquid droplets have been observed to favor reflex separation tendency over stretched droplet separation in comparison with droplets of similar liquid.<sup>12</sup> Tang *et al.*<sup>13</sup> experimentally and theoretically investigated the dynamics of the head-on collision of unequal-size droplets. Collision regimes were characterized in a  $We$ - $\Delta$  parameter space, where  $We = \rho U^2 D_f / \sigma$  for unequal-size droplets ( $D_f$  is the diameter of the smaller droplet), and  $\Delta$  is defined as the ratio of the large droplet to small droplet diameters. They established that droplet separation is suppressed in unequal-size droplet collisions due to enhanced viscous dissipation through the internal motion that helps to stabilize the coalesced droplet. Deka *et al.*<sup>14</sup> numerically investigated pinch-off dynamics and satellite droplet formation during the partial coalescence of unequal-sized droplets of the same liquid. They found that the critical diameter ratio for satellite formation rises with the increase in viscosity of both the droplet and the surrounding fluids. The oblique collision dynamics of unequal-sized liquid droplets was studied by Chaitanya *et al.*<sup>15</sup> They corroborated that the collision outcomes are affected by the asymmetric flow caused by the unequal size of droplets as well as oblique collision. While binary droplet collision has been extensively investigated in the aforementioned studies, they focused on droplet collisions in the air without the presence of a solid surface.

Several studies on the impact dynamics of a falling droplet with a solid surface have been carried out in past, although the droplet-to-droplet collision was not considered. Rioboo *et al.*<sup>16</sup> reported six impact outcomes of a droplet impacting a dry flat surface, namely, deposition, prompt splash, corona splash, receding breakup, partial rebounding, and complete rebounding. Yarin<sup>17</sup> summarized that droplet-impinging solid surfaces are complicated by surface properties, particularly wettability and roughness. For instance, for droplet impact on a hydrophobic surface, the accompanying droplet retraction on the surface can promote partial or complete rebounding.<sup>18</sup> Also, during impact, the air layer between the droplet and the solid surface can be trapped, leading to the formation of a bubble inside the droplet.<sup>19</sup> All the aforementioned studies observed that when a droplet hits a flat solid surface, it rapidly spreads circularly until it reaches the maximum spread diameter (within the splashing limit); then, retraction occurs where the spread liquid flows inwardly along the radial direction. Such spreading behavior is driven by the inertia of the droplet and opposed by the capillary and viscous forces, which can be classified into two regimes—inertial-capillary and viscous regimes.<sup>20</sup>

The maximum spread diameter of a droplet hitting a solid surface is an important parameter as it is desired to optimize the coverage of liquid over the surface. Two common analytical approaches have been developed to find the maximum spread diameter. The first approach is based on energy balance, while an effective capillary length (i.e., uses force balance) is employed in the second approach. The first approach yield that the maximum spread diameter varies as  $We^{1/2}$  when viscosity is neglected (i.e., viscous dissipation is zero), which does not agree with experimental data. The second approach predicts that the maximum spread diameter of impacting droplets varies as  $We^{1/4}$  in the inertial-capillary regime,<sup>20,21</sup> which agrees well with experimental data. When viscous dissipation was accounted for in the first approach, it also yields the same variation of the maximum spread diameter with the  $We$  number as that of the second approach. Thus, it is essential to know the viscous dissipation to use the first approach. Wildeman *et al.*<sup>21</sup> suggested a simplified way to estimate viscous

dissipation. They showed that approximately half of the kinetic energy of the falling droplet is lost as viscous dissipation in inelastic droplets collision with a flat surface (i.e., in the inertial-capillary regime). This simplification reduces the modeling effort significantly. In the viscous regime (i.e.,  $We < 1$ ), the entire kinetic energy of the falling droplet is lost as viscous dissipation and the first approach predicts that the maximum spread diameter varies as  $We^{1/5}$  (defined as  $Re = \rho U D / \mu$ , where  $\mu$  is the dynamic viscosity).<sup>20</sup> In the viscous regime, the deformation is smaller and the droplet is ellipsoidal, while the flattening of the droplet takes place in the inertial-capillary regime.<sup>22</sup>

Recently, a few studies on the dynamics of a falling droplet impacting a sessile drop have been conducted, providing useful insight into the dynamics of droplet-to-droplet impact in the presence of a solid surface. Wang *et al.*<sup>23</sup> studied the impact of a droplet with a sessile droplet on a hydrophobic substrate and observed four different regimes: coalescence, complete rebounding, coalescence accompanied by conglutination, and partial rebound after conglutination. Wakefield *et al.*<sup>24</sup> studied the coalescence of an impacting droplet with a sessile droplet on a hydrophilic surface. Damak and Varanasi<sup>25</sup> experimentally studied the maximum spread diameter and retraction rate in drop-on-drop impacts on superhydrophobic surfaces. They observed that the behavior in the receding phase of a droplet impacting onto a sessile droplet on a solid surface (after coalescence) is similar to a single droplet hitting the solid surface. Ramírez-Soto *et al.*<sup>26</sup> investigated the dynamics of an oil drop impacting an identical sessile drop sitting on a superamphiphobic surface. They observed five rebound scenarios, four of which not involving coalescence. Kumar *et al.*<sup>27</sup> experimentally investigated the coalescence dynamics of drop-on-drop impact for ethanol droplets on a hydrophilic surface. They identified two distinct coalesce regimes, namely, complete coalescence and partial coalescence. In the case of partial coalescence, the merged droplets pinched off and produced a smaller daughter droplet. Through further analyses, they found that partial coalescence occurs above a volume ratio of 2 (defined as the ratio of sessile droplet volume to falling droplet volume) and below a critical  $We$  number (1.03) at a fixed volume for the falling droplet. Jaiswal and Khandekar<sup>28</sup> investigated the drop-on-drop impact on a superhydrophobic surface both experimentally and computationally. The influence of the difference in the shape of moving droplets at the instance of impact is also analyzed. Yu *et al.*<sup>29</sup> experimentally studied the rebounding-coalescing behaviors in drop-on-drop impact on hydrophobic surfaces with varying Weber numbers and impact parameters. A regime map was proposed to show coalesce and bouncing regime. The rebounding states are divided into no-coalesce, juglike, pancake-like, and pendulum-like rebounding-coalescing behaviors. The drop-on-drop impact on solid surfaces by varying surface wettability was studied by Xing *et al.*<sup>30</sup> Chen *et al.*<sup>31</sup> established that the maximum spread diameter of merged droplets on solid surfaces increases with increasing volume ratio. Further complexities are encountered for droplets impacting heated surfaces. Guggilla *et al.*<sup>32</sup> studied the drop-on-drop impact on heated wetting surfaces. Subsequently, they also investigated the head-on impingement of a train of consecutive droplets on a heated solid surface.<sup>33</sup>

A model to predict the maximum spread diameter for the coalescence of a falling droplet with a sessile droplet was developed by Wakefield *et al.*<sup>24</sup> Since both the droplets have coalesced, the merged liquid undergoes spreading similar to spreading a droplet hitting a flat surface. Their model was based on energy balance where two distinct

methods were used to estimate viscous dissipation. In the first method, the viscous dissipation was taken as half of the kinetic energy of the falling droplet, while in the second method, it was analytically estimated by considering a simple flow inside the droplets. Predictions of the maximum spread diameter from both methods were found to agree reasonably well with the experimental data. Abouelsoud and Bai<sup>34</sup> proposed a model to predict the maximum spread diameter for the bouncing of a droplet impacting a sessile droplet. Their model too was based on energy balance, but the deformations in individual droplets are accounted for separately. They also derive an expression for the restitution coefficient during the complete bouncing. A model to predict the maximum diameter of merged droplets of equal volume on surfaces with different wettabilities was proposed by Abouelsoud *et al.*<sup>35</sup> They found that the time to attain the maximum diameter of merged droplets increases with increasing the contact angles of the sessile droplets.

The aforementioned studies on the impact of a falling droplet onto a sessile droplet were carried out either for equal-size droplets or unequal-size droplets with  $\Delta$  less than 5. Therefore, in this paper, we experimentally and theoretically investigate the dynamics of the head-on impact of two unequal-size droplets on a wetting surface with a size ratio greater than 5. The aim of this study is (1) to analyze the collision dynamics of a falling droplet with a large sessile droplet ( $\Delta > 5$ ) on a hydrophilic surface and compare with equal size droplets collision under similar situations, and (2) to develop an analytical model based on energy balance, which can predict maximum spread diameter and restitution coefficient during complete bouncing. The main difference between the current analytical model and Ref. 34 is that four stages are used to characterize the complete bouncing of unequal-size droplets in the present study, whereas only three stages are used in Ref. 34 that do not adequately characterize unequal-size droplet bouncing. The reason

for choosing  $\Delta > 5$  is (1) the effect of size ratio can be amplified due to large  $\Delta$ , and (2) the effect of solid surface on collision outcome can be reduced.

The rest of this paper is organized as follows. The experimental procedure and post-processing methods used are reported in Sec. II. In Sec. III, qualitative analyses of drop-on-drop impact based on a series of images from a high-speed camera are reported, following an analytical model to predict the maximum spread diameter and restitution coefficient of the falling droplet is also presented as well as the variation of maximum spread diameter, restitution coefficient, and contact time with  $We$  for various size ratios are analyzed. Finally, the important conclusions from this study are summarized in Sec. IV.

## II. EXPERIMENT

Figure 1 shows a schematic of the experimental apparatus used in this study. In each test, a sessile water drop is gently positioned on a solid surface using a syringe manually. Then, a smaller water droplet is generated by a droplet generator and ejects to fall on the sessile droplet. Polyvinyl chloride (PVC) is used as a solid substrate, which is a hydrophilic surface. In superhydrophobic surface, water does not spread much and water droplets bounce off upon impact (unless the weight of the droplet is high). In contrast, water on the hydrophilic surface spreads, which can cause higher viscous dissipation due to motion near the contact line. Since the sessile droplets in this study are big (large weight) and the contact line is fixed (no viscous dissipation due to contact line movement), the effect of wettability of the surface can be minimal. The droplet generator is connected to pressurized liquid water tanks in which the pressurized gas driving the liquid is regulated at 3–15 bar by a pressure regulator from SMC Co. with an accuracy of 0.1 kPa. The key component of the droplet generators is an electromagnetically controlled microvalve, SMLD-300G, produced

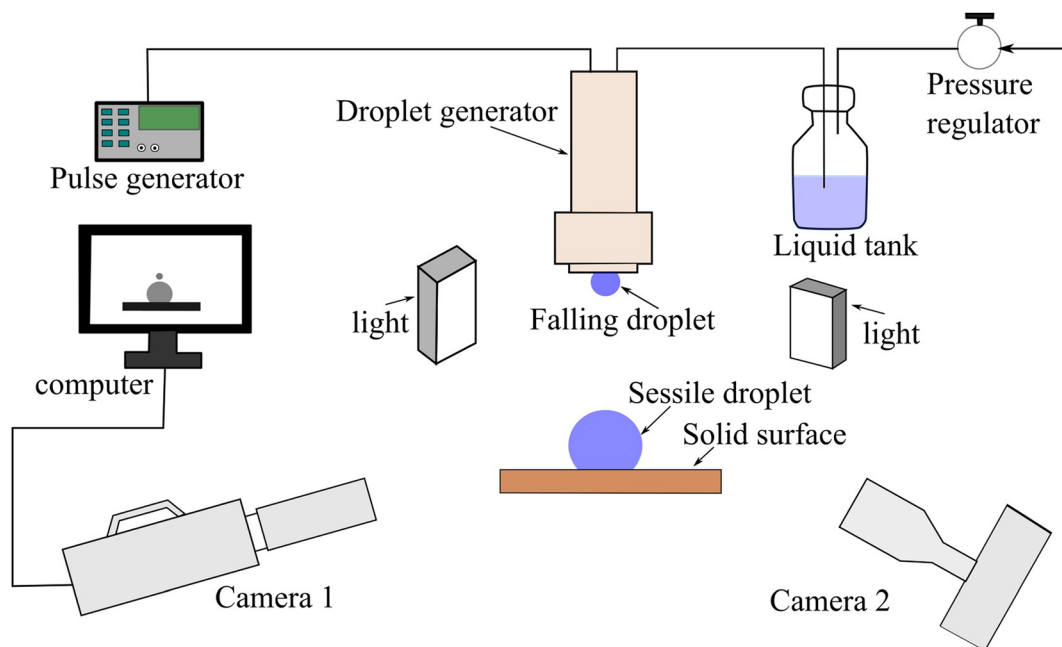


FIG. 1. Schematic of the experimental setup.

by Fritz Gyger AG. The generator has a typical response time of 400  $\mu\text{s}$  and a maximum dispensing frequency of 3000 Hz. The droplet diameter can be controlled either by changing the nozzle size of the generator valve or by changing the pressure of the pressurized liquid water tank. A single nozzle is used to carry out all the tests. The pressure difference between the water tank and the ambient affects both the diameter and impact velocity of the generated droplet. The diameter of the falling droplet lies in the range of 0.281–0.360 mm in the present study. The experimental conditions are summarized in Table I.

Two high-speed cameras are used to capture time-resolved images of the collision process. A Photron SA-Z high-speed camera mounted with a Questar QM-100 lens is used as the main camera. This camera is set to 40 000 fps with a spatial resolution of  $1024 \times 512$ . The minimum exposure time is  $O(1) \mu\text{s}$ . The second camera, Chronos 2.1 from Kron Technologies, Inc., is operated with a TCLO lens in a plane perpendicular to the previous camera and droplet trajectories plane. The second camera helps in checking the alignment of droplet impact. The fps of the second camera is set at 7135 and the spatial resolution is  $640 \times 360$ , with a minimum expose time of 10  $\mu\text{s}$ . Two lights are used as the backlight. A trigger to operate both the cameras and the droplet generators is controlled by tunable delays to ensure that the entire collision process is captured within the recording period of the camera. The recorded videos are post-processed using Photron FASTCAM viewer (PFV) and in-house scripts.

To calibrate the length in the images, a ruler with clear scale markings is first captured by the Photron SZ-A camera. Then, the value of the known length in the ruler is fed into the PFV software. After length calibration, the falling droplet diameter is determined by measuring the distance between two diametrically opposite points on the droplet. The sessile droplet diameter is estimated from the measured value of the high and base length of the sessile droplet. Travel distances can be found from a captured image by selecting two points along the falling trajectory. Distance travel by the falling droplet between a few consecutive frames is measured, which is divided by the time between the starting and ending frames to obtain the droplet velocity. The maximum spread diameter of falling droplets is determined by identified manual images of maximum distortion and measuring the maximum horizontal diameter. To determine the contact angle between the sessile droplet and the PVC surface, a circular cap is fitted to the sessile droplet and triple contact at the ends is located, and then, tangent to the circle is drawn at this point. The angle between

the tangent line and the PVC surface toward the water is the contact angle. The contact angle is then determined as the arithmetic average between the left and right contact angles.

### III. RESULTS AND DISCUSSION

#### A. Collision dynamics

To get insight into the collision dynamics of an unequal-size droplet on a wetting surface, sequential images of the collision process from the high-speed camera are analyzed. The snapshots of the droplet coalescence of a falling droplet and a sessile droplet on the solid surface are shown in Fig. 2.

Figure 2(a) (left-side images) shows coalescence at  $\Delta = 1.4$  (equal volume water droplets) on the aluminum surface at  $We = 8.0$ , where the impacting droplet has sufficient energy to drain the air layer between the two droplets to cause coalescence. The merged droplets undergo spreading to attain the maximum spread diameter, and then retract radially inward. The coalesced droplet undergoes periodic stretching in horizontal and vertical directions alternately with shorter and shorter peak deformation, until the excess energy is lost through viscous dissipation.

Figure 2(b) (Multimedia view shown at 4000 times slower) depicts the snapshots of the coalescence of a small droplet impacting a large sessile droplet on a PVC surface at  $We = 8.7$  and  $\Delta = 12.3$ . At 0.075 ms, the falling droplet is compressed and bulges, while there is no noticeable change in the shape of the sessile droplet. Then, a rim with a protrusion (capillary wave with small amplitude) is formed near the collision point at 0.175 ms. The rim widens afterward, with a crater formed at the apex of the liquid body. The formation and growth of the rim are seen in the subsequent images, where the rim moves radially outward on the surface of the coalesced droplet with a cavity at the center. The contact angle between the sessile droplet and the PVC surface does not change until the ripple arrives near the contact line. The contact line is pinned in Fig. 2(b), while for drop-on-drop impact with similar droplet sizes, as shown in Fig. 2(a), it moves significantly during the coalescence process. It is also interesting to note that the coalesced droplet does not undergo prominent spreading or retraction as in Fig. 2(a). Instead, a ripple travels smoothly on the sessile droplet surface. After sufficient time, the disturbance caused by the collision is damped by viscous dissipation and the coalesced droplet attains a spherical cap shape.

Figure 3 shows the representative sequential images of droplets bouncing when a falling droplet impacts a sessile droplet at different size ratios. Figure 3(a) exhibits bouncing at  $\Delta = 1.4$  (equal volume of the droplets), while Fig. 3(b) has  $\Delta = 7.2$ . From Fig. 2(a), it can be seen that when the falling droplet impacts the sessile droplet, both droplets are deformed into a disk shape at maximum deformation. The energy of the impacting droplet is not sufficient to drain the air layer between them and thus bouncing occurs. Owing to the loss of energy of falling droplets due to viscous dissipation, the value of rebound velocity is smaller than impact velocity.

The bouncing of two colliding droplets at a large size ratio is shown in Fig. 3(b) (Multimedia view). When the falling droplet impacts the sessile droplet, the falling droplet motion is opposed, forcing it to stretch radially. At this time, the sessile droplet also deforms, but only locally near the impact area, and the falling droplet intrudes partially inside it while expanding radially. At 0.250 ms, the falling droplet attains maximum horizontal diameter, whereas the sessile

TABLE I. Experimental conditions studied in this work and Abouelsoud and Bai.<sup>34</sup>

Parameter	This study	Ref. 34
Falling droplet diameter (mm)	0.281–0.360	2.680–2.779
Sessile droplet diameter (mm)	2.290–2.980	3.880–4.000
Static contact angle (deg)	67.3–78.0	73.0–81.0
Size ratio, $\Delta$	7.2–12.3	1.4
Weber number, $We$	3.7–9.2	2.7–8.0
Ohnesorge number, $Oh$	$6.2 \times 10^{-3}$ – $7.0 \times 10^{-3}$	$2.2 \times 10^{-3}$ – $2.3 \times 10^{-3}$
Reynolds number, $Re$	281–461	713–1208



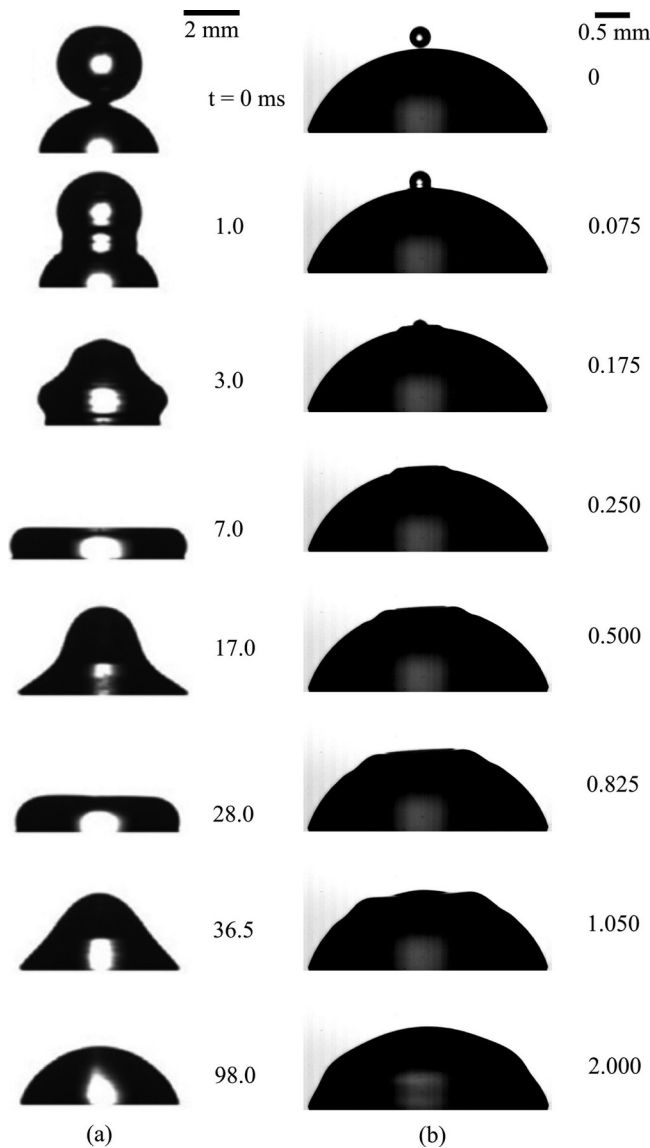


**FIG. 2.** Photographic images showing representative sequences of coalescence for water droplet collisions with greatly different  $\Delta$ . (a)  $(We, \Delta, \theta) = (8.0, 1.4, 77.0)$  (Abouelsoud and Bai<sup>34</sup>) and (b)  $(We, \Delta, \theta) = (8.7, 12.3, 67.3)$  (present study). Multimedia view: <https://doi.org/10.1063/5.0139663.1>

droplet is significantly less deformed. Following this, the falling droplet starts to retract and move upward, while the sessile droplet continues to deform. At 0.850 ms, maximum vertical deformation of the sessile droplet is reached, which is followed by the complete bouncing of the falling droplet at around 1.125 ms. During the entire collision process, the deformation in the sessile droplet only occurs locally near the impact region, and the contact angle between the sessile droplet and the PVC surface does not change significantly with a fixed contact line. When the falling droplet is partially immersed in the sessile droplet during impact, it is not clear whether the droplets merge or remain separated. To clarify this point, a critical case that lies between the

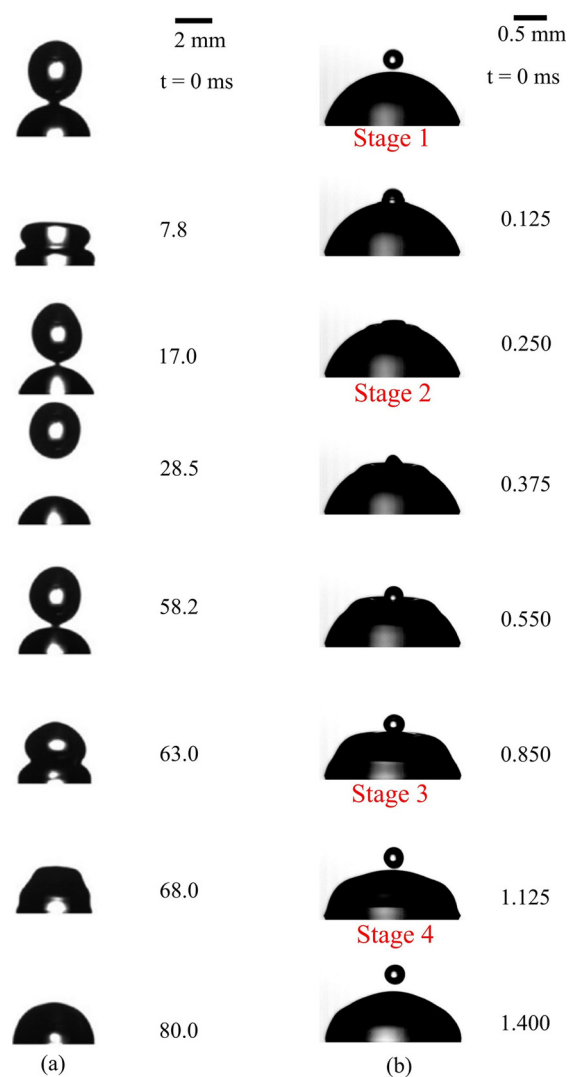


**FIG. 3.** Photographic images showing representative sequences of bouncing for water droplet collisions with greatly different  $\Delta$ . (a)  $(We, \Delta, \theta) = (2.7, 1.4, 77.0)$  (Abouelsoud and Bai<sup>34</sup>) and (b)  $(9.2, 7.2, 72.6)$  (present study). Stages 1 to 4 are labeled below the sessile droplets and are defined in Fig. 5. Multimedia view: <https://doi.org/10.1063/5.0139663.2>

coalescence and bouncing regimes and is referred to here as partial coalescence–partial bouncing is analyzed further.

Figure 4 (Multimedia view) shows the representative sequential images of the partial coalescence–partial bouncing of an impacting droplet with a larger sessile droplet. The collision sequences are similar to the bouncing case in Fig. 3(b) until 0.975 ms, and at this time instance, both the droplets are connected at the apex by a small liquid column. It is interesting to note that the falling droplet does not completely bounce, but rather remains attached to the sessile droplet. The contact body between the droplets grows hereafter and quickly widens as a liquid neck. The water from the falling droplet is drained into the sessile droplet through the liquid neck. Thereafter, the

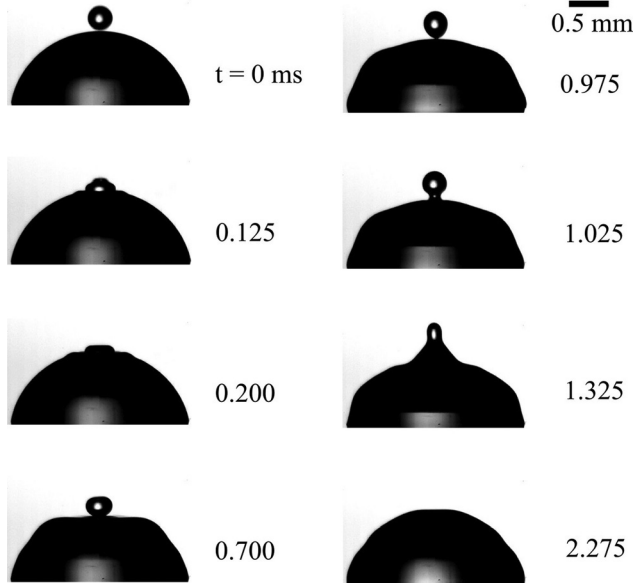


**FIG. 4.** Photographic images showing representative sequences of partial coalescence–partial bouncing for water droplet collisions.  $(We, \Delta, \theta) = (7.3, 7.5, 76.5)$ . Multimedia view: <https://doi.org/10.1063/5.0139663.3>.

droplets coalesce and eventually attain a spherical cap shape. It is clear from these image sequences that partial coalescence–partial bouncing lies between coalescence and bouncing regimes. Thus, reflex separation (mentioned in Sec. I) does not occur in the range of the  $We$  number (3.7–9.2) in the present study. This means that the water from falling droplets does not mix with water in the sessile droplet during the bouncing of the droplets.

## B. Bouncing characteristic

To better characterize the bouncing observed in Fig. 3 and the underlying principles, further analysis is conducted. A schematic summarizing the representative stages during bouncing from a larger droplet is presented in Fig. 5. Stages 1, 2, 3, and 4 represent the beginning of the impact, the maximum horizontal spreading of the falling droplet, maximum distortion of the sessile droplet, and complete rebounding, respectively. Several assumptions are made during the energy balance analysis: (1) the collision of droplets is head-on, (2) the falling droplet has a spherical shape before and after the collision without any internal circulation, (3) the shape of the sessile droplet is that of the spherical cap before the collision as the Bond number is less than one, (4) no mass is exchanged between the droplets during impact, and (5) the exchange of energy between the droplets is negligible after the falling droplet reaches a maximum spread diameter.

The maximum spread diameter of the falling droplet can be found via energy balance between stage 1 and stage 2 (see Fig. 5). For stage 1, the falling droplet just began to impact the sessile droplet with the kinetic energy  $E_{kf1} = \frac{1}{12}\pi\rho D_f^3 U^2$ , and the surface energy  $E_{sf1} = \pi D_f^2 \sigma$ , while the sessile droplet has the surface energy  $E_{ss1} = \frac{\pi}{4} B_s^2 (1 - \cos \theta_1) \sigma + \pi \left( \frac{B_s^2}{4} + h_s^2 \right) \sigma$  and no kinetic energy. Here,  $E$

stands for energy,  $B_s$  is the base diameter of the sessile droplet, and  $h_s$  is the height of the sessile droplet. The subscripts  $K, S, f, s$ , and  $l$  stand for the kinetic energy, the surface energy, the falling drop, the sessile drop, and stage 1, respectively. The first term in the surface energy of the sessile droplet is due to contact of the bottom side of the sessile droplet with the solid surface and contains  $\theta$ .<sup>36</sup> The second term is due to the top surface exposure to the air. The kinetic energy comprised two parts: the first part is due to translational motion of the center of mass, and the second part is due to the rotational motion about the center of mass. Following assumption (2), the contribution to the kinetic energy due to internal motion in the falling droplet is zero at stage 1 and stage 4. In stage 2, the kinetic energy of the falling droplet is zero as the velocity is zero due to flow reversal occurring. The horizontal diameter and height of the falling droplet are  $D_{max,f}$  and  $h_{f2}$ , respectively. The surface energy of the falling droplet is  $E_{sf2} = (\pi D_{max,f} h_{f2} + \frac{\pi}{2} D_{max,f}^2) \sigma$ . In contrast, the sessile droplet has not reached the maximum deformation and significant flow may exist inside it. Thus, the kinetic energy ( $E_{ks2}$ ), due to internal motion inside the sessile droplet, is finite. The volume of the falling droplet is fixed as mass exchange does not take place between the droplets in the case of bouncing. The energy balance for stage 1 and stage 2 can be written as follows:

$$E_{kf1} + E_{sf1} + E_{ss1} = E_{sf2} + E_{ss2} + E_{ks2} + E_{diss1-2}, \quad (1)$$

where  $E_{diss1-2}$  is the viscous dissipation from stage 1 to stage 2. The viscous dissipation term in Eq. (1) is estimated similarly as employed in Ref. 34 and given by  $E_{diss1-2} = \frac{1}{24} \pi \rho D_f^3 U^2$ . The maximum deformation of the sessile droplet occurs at stage 3. The sessile droplet surface area is estimated by considering it as a truncated cone as the shape of the sessile droplet resembles close to a truncated cone in our experiments [see Fig. 3(b)]. The surface energy of the sessile droplet at stage 3 is  $E_{ss3} = A_{s3} \sigma + \frac{\pi}{4} B_s^2 (1 - \cos \theta_3) \sigma$ , where  $A_{s3}$  and  $l_s$  are the surface area of the slanted surface plus the top surface and slant height of the sessile droplet at stage 3, respectively, and given as  $A_{s3} = \frac{\pi}{4} b_s^2 + \pi l_s \left( \frac{B_s}{2} + \frac{h_{s3}}{2} \right)$ , and  $l_s = \sqrt{h_{s3}^2 + (B_s - b_s)^2 / 4}$ . Following assumption (5), the energy balance between stages 2 and 3 for the sessile droplet is given by

$$E_{ss3} \approx E_{ss2} + E_{ks2}. \quad (2)$$

An implicit expression for the dimensionless maximum spread diameter is obtained as follows. First, Eq. (2) is used to eliminate  $E_{ss2}$  and  $E_{ks2}$  from Eq. (1). The expression for each term is plugged in Eq. (1). Then,  $\pi D_f^2 \sigma$  is divided throughout Eq. (1) and terms are rearranged to write the expression in terms of dimensionless terms. The derived implicit expression for the dimensionless maximum spread diameter is given by

$$\frac{We}{24} + 1 + \frac{\lambda^2}{4} (1 - \cos \theta_1) + \left( \frac{\lambda^2}{4} + \delta^2 \right) = \left( \frac{2}{3C\beta_{max,f}} + \frac{C^2 \beta_{max,f}^2}{4} \right) + \frac{A_{s3}}{\pi D_f^2} + \frac{\lambda^2}{4} (1 - \cos \theta_3), \quad (3)$$

where  $\lambda = \frac{B_s}{D_f}$ ,  $\delta = \frac{h_s}{D_f}$ ,  $\beta_{max,f} = \frac{D_{max,f}}{D_f}$ ,  $A_s$  is sessile droplet surface area, and  $\theta_1$ ,  $\theta_2$ , and  $\theta_3$  are the contact angles at stage 1, stage 2, and stage 3, respectively. The experimentally determined values of contact angles

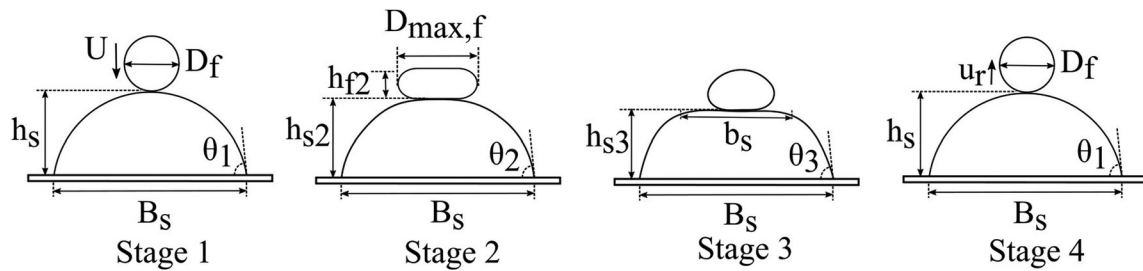


**FIG. 5.** Representative stages during bouncing of the falling droplet: stage 1 the first impact, stage 2 the maximum spreading of the falling droplet, stage 3 the maximum deformation of the sessile droplet, and stage 4 rebounding.

are used in the model. A correction factor  $C$  with a value of 0.90 is used in Eq. (3).

The restitution coefficient ( $\varepsilon$ ) of the falling droplet is the ratio of bouncing velocity ( $u_r$ ) to impacting velocity ( $U$ ). To find an expression for the restitution coefficient, the energy balance for falling droplets at stage 2 and stage 4 is equated

$$E_{sf2} \approx E_{sf4} + E_{kf4}. \quad (4)$$

At stage 4, the surface energy of the falling droplet is  $E_{sf4} = E_{sf1} = \pi D_f^2 \sigma$  and the kinetic energy of the falling droplet is  $E_{kf4} = \frac{1}{12} \pi \rho D_f^3 u_r^2$ . After substituting the expressions for  $E_{sf2}$ ,  $E_{sf4}$ , and  $E_{kf4}$  in Eq. (4) and rearranging for  $\frac{U}{u_r}$  (i.e.,  $\varepsilon$ ), we get the restitution coefficient as

$$\varepsilon = C_0 \sqrt{12 \left( \frac{4D_f^3 + 3d_{\max,f}^3}{6D_f^2 d_{\max,f}} - 1 \right) / We}. \quad (5)$$

In Eq. (5),  $C_0$  is a correction factor obtained by fitting our experimental data. The value of  $C_0$  obtained is 0.45. The length and velocity scales used to calculate the  $We$  number in Eq. (5) are the falling droplet diameter and velocity at stage 1, respectively.

Figure 6 shows the maximum spread diameter of the falling droplets as a function of  $We$ . Three datasets are included for comparison, namely, our experimental data, and the experimental data reported in Abouelsoud and Bai,<sup>34</sup> and calculated values from Eq. (3). It can be seen that the maximum spread diameter does not change significantly with increasing  $We$  in the bouncing regime. It is interesting

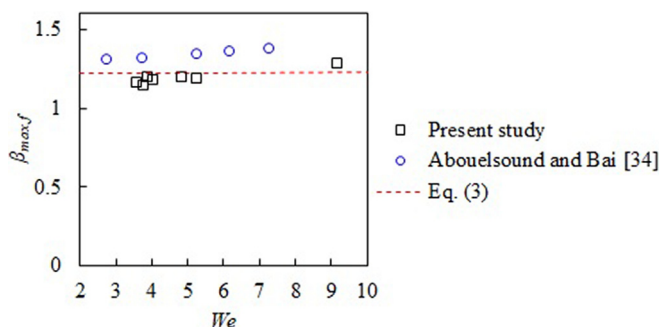


**FIG. 6.** Dimensionless maximum spread diameter of the falling droplet as a function of  $We$ .

to note that the maximum spread diameter is smaller for a large size ratio compared to near unity size ratio. This could be due to better transfer of energy from impacting droplet to another droplet during the spreading phase when the size of the other droplet is much bigger relative to impacting droplet. The predictions of maximum spread diameter by the model also show that it does change with the  $We$  number. The agreement between the modeled and experimental values of the maximum spread diameter is quite good.

The calculated restitution coefficients ( $\varepsilon$ ) from Eq. (5) are shown in Fig. 7 (log-log plot) as a function of  $We$ , along with the experimental data from the present study and Ref. 34. It can be seen that  $\varepsilon$  decreases with increasing  $We$ . This could be attributed to the higher viscous dissipation at a higher impact Weber number due to the violent deformation of the falling droplet, leaving less energy to bounce the falling droplet up. It is noteworthy that the calculated and experimental results agree well with each other, qualitatively in the decreasing trend of  $\varepsilon$  with  $We$ . Also noteworthy is that  $\varepsilon$  scales with  $We$  irrespective of size ratio, at a rate of approximately  $We^{-1/2}$ , according to Eq. (5). Previous studies showed that the impact of a droplet onto a superhydrophobic surface is highly elastic with a high  $\varepsilon$  value (0.7–1.0). In contrast, the impact of a droplet onto a hydrophilic surface is inelastic with a lower  $\varepsilon$  value due to higher viscous dissipation.<sup>22,37,38</sup> At a larger size ratio, the viscous dissipation is more, but no noticeable change in  $\varepsilon$  values is observed. The bigger sessile droplet causes (1) increased viscous dissipation due to bigger droplet size, (2) a decrease in the deceleration of falling droplet (see Fig. 8, which shows longer contact time at higher size ratio) and the deformation of the sessile droplet can store more energy (i.e., both the surface and kinetic

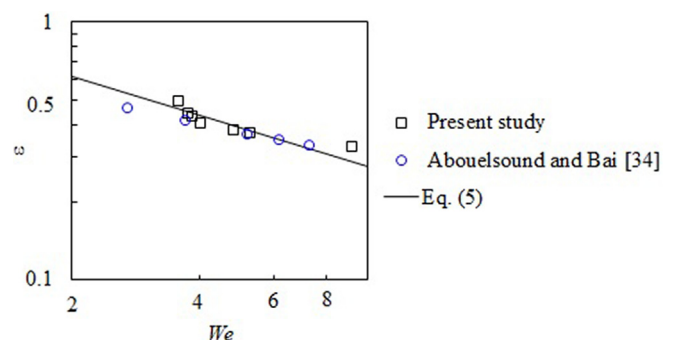


**FIG. 7.** The restitution coefficient of the falling droplet as a function of  $We$ .



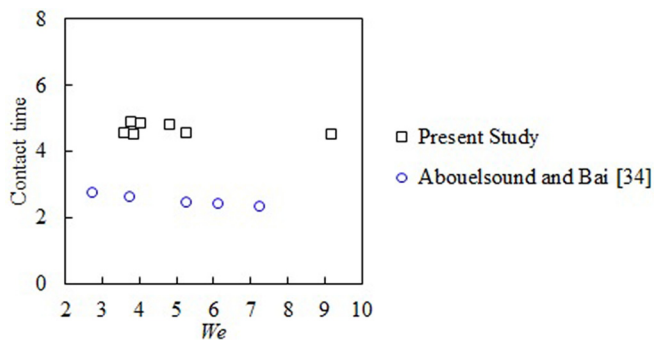


FIG. 8. Dimensionless contact time as a function of  $We$ .

energy). Both the effects are balanced resulting in similar values of  $\varepsilon$  at different size ratios for a fixed  $We$ .

Figure 8 shows the dimensionless contact time for complete bouncing during drop-on-drop impact as a function of  $We$ . Here, contact time is non-dimensionalized with the inertial-capillary time scale [ $t_c = (\rho R_f^3 / \sigma)^{1/2}$ , where  $R_f$  is the radius of the falling droplet]. It can be seen from Fig. 8 that the contact time during bouncing is almost constant with  $We$ . At a large size ratio, the contact time is longer compared with size ratio near one. The longer contact time at a higher size ratio is due to a decrease in deceleration of the falling droplet by a bigger sessile droplet. In contrast, the contact time for the bouncing of a droplet impacted onto a superhydrophobic surface is 2.6 times the inertial-capillary time scale regardless of  $We$ .<sup>39,40</sup>

#### IV. CONCLUSIONS

The collision dynamics of the head-on impact of unequal-size droplets on a wetting surface have been investigated experimentally and theoretically at various size ratios (1.4–12.3) and relatively low impact Weber numbers (2.7–9.2). A series of images of droplet collision sequences from the high-speed digital camera are compared at different size ratios for similar situations. Different collision outcomes such as coalescence, bouncing, and partial coalescence–partial bouncing are captured and analyzed. The key differences in impact behaviors observed are (1) the merging of a falling droplet with a much bigger sessile droplet occurs in a local region, whereas entire surfaces of droplets are modified during merging of equal size droplets; (2) a capillary wave with small amplitude ( $\ll$  sessile droplet radius) is generated during coalesce at high size ratio, which move radially outward on the sessile droplet surface, whereas the amplitude of capillary wave is much higher (on the order of droplet radius) for small size ratio such that the coalesced droplet experiences huge deformation; (3) the falling droplet is partially immersed inside the sessile droplet during bouncing at higher size ratios ( $>5$ ), while immersing of falling droplet is absent at low size ratios; (4) with large size ratios, the maximum deformation in the sessile droplet occurs at a later time than the maximum deformation of the falling droplet, whereas both the droplets attain maximum deformation at same time instance for near unity size ratio; and (5) the contact line is pinned and does not change much until a later time when capillary wave arrives near the contact line for large size ratio.

Four different stages are identified in the bouncing process. Subsequently, an analytical model is developed based on energy balance. The model is successfully demonstrated by predicting the dimensionless maximum spread diameter ( $\beta_{max,f}$ ) and restitution coefficient ( $\varepsilon$ ) of the falling droplet for various bouncing situations, where good agreement between the model and experimental data is obtained. Particularly, the restitution coefficient does not change significantly at a higher size ratio despite more viscous dissipation in bigger sessile droplets and the restitution coefficient scales with  $We^{-1/2}$ . The developed model can guide the design of applications involving unequal-size droplet collision on a surface, such as precisely controlling the spreading of droplets hitting other droplets in inkjet printing, and properly selecting parameters in agricultural sprays such that chemicals stick on leaves.

#### ACKNOWLEDGMENTS

The work described in this paper was supported by grants from the Research Grants Council of the Hong Kong Special Administrative Region, China (Nos. CityU 15222421, CityU 15218820, PolyU P0034937, and PolyU P0039589).

#### AUTHOR DECLARATIONS

##### Conflict of Interest

The authors have no conflicts to disclose.

#### Author Contributions

**Saroj Ray:** Conceptualization (equal); Formal analysis (equal); Investigation (equal); Methodology (equal); Software (equal); Writing – original draft (equal); Writing – review & editing (equal). **Yicheng Chi:** Investigation (supporting); Methodology (equal). **Peng Zhang:** Conceptualization (equal); Funding acquisition (equal); Project administration (equal); Supervision (equal); Writing – original draft (equal); Writing – review & editing (equal). **Song Cheng:** Conceptualization (equal); Formal analysis (equal); Funding acquisition (equal); Project administration (equal); Supervision (equal); Writing – original draft (equal); Writing – review & editing (equal).

#### DATA AVAILABILITY

The data that support the findings of this study are available from the corresponding author upon reasonable request.

#### REFERENCES

- V. Bergeron, D. Bonn, J. Y. Martin, and L. Vovelle, “Controlling droplet deposition with polymer additives,” *Nature* **405**, 772 (2000).
- R. J. Gilliom, J. E. Barbash, C. G. Crawford, P. A. Hamilton, J. D. Martin, N. Nakagaki, L. H. Nowell, J. C. Scott, P. E. Stackelberg, and G. P. Thelin, “Pesticides in the nation’s streams and ground water 1992–2001,” Circular Report No. 1291, The Quality of Our Nation’s Waters (U.S. Geological Survey, 2006), p. 184.
- M. Massinon and F. Lebeau, “Comparison of spray retention on synthetic superhydrophobic surface with retention on outdoor grown wheat leaves,” in *Proceedings of the Aspects 114 International Advances in Pesticide Application* (Association of Applied Biologists, Warwick, United Kingdom, 2012).
- H. Wijnshoff, “The dynamics of the piezo inkjet printhead operation,” *Phys. Rep.* **491**(4–5), 77 (2010).

- <sup>5</sup>J. Z. Wang, Z. H. Zheng, H. W. Li, W. T. S. Huck, and H. Sirringhaus, "Dewetting of conducting polymer inkjet droplets on patterned surfaces," *Nat. Mater.* **3**(3), 171 (2004).
- <sup>6</sup>D. Soltman and D. V. Subramanian, "Inkjet-printed line morphologies and temperature control of the coffee ring effect," *Langmuir* **24**(5), 2224 (2008).
- <sup>7</sup>J. Adam, N. Lindblad, and C. Hendricks, "The collision, coalescence, and disruption of water droplets," *J. Appl. Phys.* **39**(11), 5173 (1968).
- <sup>8</sup>N. Ashgriz and J. Poo, "Coalescence and separation in binary collisions of liquid drops," *J. Fluid Mech.* **221**, 183 (1990).
- <sup>9</sup>Y. J. Jiang, A. Umemura, and C. K. Law, "An experimental investigation on the collision behavior of hydrocarbon droplets," *J. Fluid Mech.* **234**, 171 (1992).
- <sup>10</sup>J. Qian and C. K. Law, "Regimes of coalescence and separation in droplet collision," *J. Fluid Mech.* **331**, 59 (1997).
- <sup>11</sup>K. L. Pan, P. C. Chou, and Y. J. Tseng, "Binary droplet collision at high Weber number," *Phys. Rev. E* **80**(3), 036301 (2009).
- <sup>12</sup>R. H. Chen, "Diesel-diesel and diesel-ethanol drop collisions," *Appl. Therm. Eng.* **27**(2–3), 604 (2007).
- <sup>13</sup>C. Tang, P. Zhang, and C. K. Law, "Bouncing, coalescence, and separation in head-on collision of unequal-size droplets," *Phys. Fluids* **24**(2), 022101 (2012).
- <sup>14</sup>H. Deka, G. Biswas, S. Chakraborty, and A. Dalal, "Coalescence dynamics of unequal sized drops," *Phys. Fluids* **31**(1), 012105 (2019).
- <sup>15</sup>G. S. Chaitanya, K. C. Sahu, and G. Biswas, "A study of two unequal-sized droplets undergoing oblique collision," *Phys. Fluids* **33**(2), 022110 (2021).
- <sup>16</sup>R. Rioboo, C. Tropea, and M. Marengo, "Outcomes from a drop impact on solid surfaces," *Atomization Sprays* **11**(2), 155 (2001).
- <sup>17</sup>A. L. Yarin, "Drop impact dynamics: Splashing, spreading, receding, bouncing," *Annu. Rev. Fluid Mech.* **38**(1), 159 (2006).
- <sup>18</sup>Y. Renardy, S. Popinet, L. Duchemin, M. Renardy, S. Zaleski, C. Josserand, M. A. Drumright-Clarke, D. Richard, C. Clanet, and D. Quéré, "Pyramidal and toroidal water drops after impact on a solid surface," *J. Fluid Mech.* **484**, 69 (2003).
- <sup>19</sup>C. Josserand and S. T. Thoroddsen, "Drop impact on a solid surface," *Annu. Rev. Fluid Mech.* **48**(1), 365 (2016).
- <sup>20</sup>C. Clanet, C. Béguin, D. Richard, and D. Quéré, "Maximal deformation of an impacting drop," *J. Fluid Mech.* **517**, 199 (2004).
- <sup>21</sup>S. Wildeman, C. W. Visser, C. Sun, and D. Lohse, "On the spreading of impacting drops," *J. Fluid Mech.* **805**, 636 (2016).
- <sup>22</sup>D. Richard and D. Quéré, "Bouncing water drops," *Europhys. Lett.* **50**(6), 769 (2000).
- <sup>23</sup>F. C. Wang, J. T. Feng, and Y. P. Zhao, "The head-on colliding process of binary liquid droplets at low velocity: High-speed photography experiments and modeling," *J. Colloid Interface Sci.* **326**(1), 196 (2008).
- <sup>24</sup>J. Wakefield, C. F. Tilger, and M. A. Oehlschlaeger, "The interaction of falling and sessile drops on a hydrophobic surface," *Exp. Therm. Fluid Sci.* **79**, 36 (2016).
- <sup>25</sup>M. Damak and K. Varanasi, "Expansion and retraction dynamics in drop-on-drop impacts on nonwetting surfaces," *Phys. Rev. Fluids* **3**(9), 093602 (2018).
- <sup>26</sup>O. Ramírez-Soto, V. Sanjay, D. Lohse, J. T. Pham, and D. Vollmer, "Lifting a sessile oil drop from a superamphiphobic surface with an impacting one," *Sci. Adv.* **6**(34), eaba4330 (2020).
- <sup>27</sup>M. Kumar, R. Bhardwaj, and K. C. Sahu, "Coalescence dynamics of a droplet on a sessile droplet," *Phys. Fluids* **32**(1), 012104 (2020).
- <sup>28</sup>A. K. Jaiswal and S. Khandekar, "Drop-on-drop impact dynamics on a superhydrophobic surface," *Langmuir* **37**(43), 12629 (2021).
- <sup>29</sup>W. Yu, D. Zhu, W. Wang, Z. Yu, S. Chen, and J. Zhao, "The rebounding-coalescing behaviors in drop-on-drop impact on a superhydrophobic surface," *Appl. Phys. Lett.* **121**(6), 061602 (2022).
- <sup>30</sup>A. L. Xing, B. J. Li, C. M. Jiang, and D. L. Zhao, "Simulation of coalescence dynamics of droplets on surfaces with different wettabilities," *Phys. Fluids* **34**(7), 072114 (2022).
- <sup>31</sup>D. Chen, T. Wang, L. Ming, M. Qiu, and Z. Lin, "Dynamic characteristics of moving droplets impacting sessile droplets with different Reynolds numbers," *Phys. Fluids* **34**(11), 117120 (2022).
- <sup>32</sup>G. Guggilla, A. Pattamatta, and R. Narayanaswamy, "Numerical investigation into the evaporation dynamics of drop-on-drop collisions over heated wetting surfaces," *Int. J. Heat Mass Transfer* **123**, 1050 (2018).
- <sup>33</sup>G. Guggilla, R. Narayanaswamy, P. Stephan, and A. Pattamatta, "Influence of flow rate and surface thickness on heat transfer characteristics of two consecutively impinging droplets on a heated surface," *Int. J. Heat Mass Transfer* **165**, 120688 (2021).
- <sup>34</sup>M. Abouelsoud and B. Bai, "Bouncing and coalescence dynamics during the impact of a falling drop with a sessile drop on different solid surfaces," *Phys. Fluids* **33**(6), 063309 (2021).
- <sup>35</sup>M. Abouelsoud, V. A. Thale, A. N. Shmroukh, and B. Bai, "Spreading and retraction of the concentric impact of a drop with a sessile drop of the same liquid: Effect of surface wettability," *Phys. Fluids* **34**(11), 112108 (2022).
- <sup>36</sup>P. G. De Gennes, F. Brochard-Wyart, and D. Quéré, *Capillarity and Wetting Phenomena: Drops, Bubbles, Pearls, Waves* (Springer, New York, 2004).
- <sup>37</sup>A. L. Biance, F. Chevy, C. Clanet, G. Lagubeau, and D. Quéré, "On the elasticity of an inertial liquid shock," *J. Fluid Mech.* **554**, 47 (2006).
- <sup>38</sup>C. Hao, J. Li, Y. Liu, X. Zhou, Y. Liu, R. Liu, R. Che, W. Zhou, D. Sun, L. Li, L. Xu, and Z. Wang, "Superhydrophobic-like tunable droplet bouncing on slippery liquid interfaces," *Nat. Commun.* **6**(1), 7986 (2015).
- <sup>39</sup>D. Richard, C. Clanet, and D. Quéré, "Contact time of a bouncing drop," *Nature* **417**(6891), 811 (2002).
- <sup>40</sup>A. Gauthier, S. Symon, C. Clanet, and D. Quéré, "Water impacting on superhydrophobic macrottextures," *Nat. Commun.* **6**(1), 8001 (2015).